sustainability

MDPI

Article

Comparison of Potential Contribution of Typical Pavement Materials to Heat Island Effect

Hailu Yang [1], Kai Yang [1], Yinghao Miao [1,*], Linbing Wang [2,*] and Chen Ye [1]

[1] National Centre for Materials Service Safety, University of Science & Technology Beijing, Beijing 100083, China; yanghailu@ustb.edu.cn (H.Y.); s20151203@ustb.cn (K.Y.); g20178999@xs.ustb.edu.cn (C.Y.)

[2] Joint USTB Virginia Tech Lab on Multifunctional Materials, Department Civil & Environmental Engineering, Virginia Tech, Blacksburg, VA 24061, USA

* Correspondence: miaoyinghao@ustb.edu.cn (Y.M.); wangl@vt.edu (L.W.)

Received: 24 April 2020; Accepted: 7 June 2020; Published: 10 June 2020

Abstract: Pavement materials have significant influence on the urban heat island effect (UHIE). This paper presents a study on the potential effects of pavement materials on UHIE in a natural environment. Three typical pavement materials, including cement concrete, dense asphalt concrete and porous asphalt mixture, were selected to evaluate their anti-UHIE properties by testing. In this paper, heat island potential (HIP) is proposed as a new index to analyze the influence of pavement materials on UHIE. It is shown that the temperature inside a pavement distinctly depends on the depth, and varies, but is usually higher than the air temperature. Solar radiation in the daytime significantly contributes to the temperature of pavement surface and the upper part. The correlation becomes weak at the middle and the bottom of pavements. Among the three materials tested in this study, the anti-UHIE performance of cement concrete is significantly higher than that of the other asphalt mixtures, while the porous asphalt mixture is slightly better than the dense asphalt concrete in anti-UHIE.

Keywords: urban heat island; asphalt concrete mixture; cement concrete mixture; porous asphalt concrete mixture

1. Introduction

Concrete materials are the most widely used in urban infrastructure. The materials should comply with the principles of sustainability [1–3] and be friendly to climate and environment. The urban heat island effect (UHIE) is defined as the temperature difference between rural and urban areas that is mainly caused by urban construction and intense human activities. It is shown that the annual average temperature of urban areas is 0.5–3 °C higher than that of the suburbs, and even 6 °C higher during summer [4–6]. UHIE has been considered as one of the major problems in urbanization and industrialization of human civilization [7]. It has increased the occurrences of extreme weather such as heavy precipitation and storms [8,9], accelerated global warming, raised the energy demand of cities [10–12], elevated environmental pollution, damaged human health, and even contributed to mortality rates [13,14].

UHIE is a natural imbalance due to human activities. Natural underlying surfaces with good cooling capacity have decreased gradually with urban development while artificial underlying surfaces with poor heat dissipation have continuously increased, which has resulted in an increase in the amount of heat stored in the urban system. Civil engineering materials such as cement concrete and asphalt concrete have been widely used in urban road construction, and bring remarkable features such as high-absorptivity, low-calorific capacity and impermeability [15]. The thermal properties of pavements make a significant contribution to UHIE.

The external environment and pavement characteristics are the major factors that influence the pavement temperature field. There is natural convection between pavement and the external environment [16]. Thermal radiation transfer also occurs, which includes mainly solar radiation during the daytime and atmospheric long-wave radiation [17,18]. Environmental conditions such as air temperature, solar radiation, wind speed and other factors are difficult to control, so researchers adjusted pavement characteristics to ease UHIE. Obviously, the performance of pavement materials plays an important role, which affects the internal temperature variation and heat transfer capacity of the pavement [19].

Many measures have been tried to control the UHIE through improving the performance of pavement materials. High-albedo coating is verified as an effective anti-UHIE technology, which can lower the pavement temperature by increasing the solar-reflective rate of pavements [20,21]. Some materials such as water-cooled, porous and thermal resistance materials were also developed to improve stability of pavement temperature [22,23]. Some researchers have developed new materials to moderate the thermal conditions of pavements through promoting the evaporation and the water exchange between ground surface and deep soil [24,25]. For instance, porous materials can help alleviate heat accumulation [26] because the strong drainage performance of the porous materials can significantly lower the pavement's thermal conductivity [27].

Understanding the potential contributing effects of pavement materials to UHIE is helpful in making reasonable choices in pavement design. This paper presents a study focusing on how pavement materials affect UHIE in a natural environment. Three typical pavement materials—cement concrete, dense asphalt concrete and porous asphalt mixture—were selected to evaluate their temperature variation in the natural environment where the temperature is constantly changing. The effects of these commonly used pavement materials on UHIE were compared according to the experimental results.

2. Materials and Methods

Three types of pavement materials were selected for the test. The pavement materials were a cement concrete (C25, P.O 42.5), a porous asphalt mixture (PAC13, 90#, 20%) and a dense asphalt concrete (AC13, 90#).

The raw materials of the cement concrete included water, Portland cement (Type 42.5), sand, limestone and additives. The raw materials of the asphalt concrete included limestone powder, limestone, 90# petroleum asphalt and high viscosity modified asphalt. The mix proportions of the three specimens are shown in Tables 1–3, respectively.

Table 1. Mix proportions of cement concrete (C25).

w/c Ratio	Mass (kg/m^3)					
	Water	Cement	Sand	Coarse Aggregate	Fly Ash	Super-Plasticizer
0.55	265	150	872	1061	33	1.3

Table 2. Mix proportions of dense asphalt concrete (AC13).

Asphalt-Aggregate Ratio	Mass Ratio				
	Mineral Powder	0~2.36	2.36~5	5~10	10~15
5.0%	0.05	0.3	0.11	0.24	0.3

Table 3. Mix proportions of porous asphalt concrete specimen (PAC13).

Asphalt-Aggregate Ratio	Mass Ratio			
	Mineral Powder	0~3	5~10	10~15
4.8%	0.04	0.1	0.34	0.52

The volume indexes of asphalt mixture AC13 and PAC13 including asphalt content (AC), air void content (AV), voids in mineral aggregate (VMA), and voids filled with asphalt (VFA) are shown in Table 4.

Table 4. The volume index of asphalt mixture.

Asphalt Mixture Type	AC %	AV %	VMA %	VFA %
AC13	4.8	4.4	16.1	73.0
PAC13	4.6	19.1	27.8	31.3

The production process of the cement concrete was as follows: firstly, according to the proportion, add cement, sand and aggregates into the mixer to mix evenly, and then add water to mix evenly. Then, take out the mixture and put it into the mold, place the mold on the vibration table to vibrate and smooth the surface. Finally, after it had been cured in the laboratory for 24 h, the specimens were demolded and placed in the standard curing room with 20 ± 3 °C and 95% relative humidity for 28 days.

The production process of the asphalt concrete was as follows: firstly, put all kinds of mineral materials in 105 °C oven and dry for 6 h. Secondly, the dry graded coarse and fine aggregates are weighed according to the design grading requirements, mixed evenly in a metal plate, the mineral powder shall be placed in a metal basin, and then heated to 165 °C in an oven. Take the specified weight of asphalt and heat it to 150 °C in an oven. Thirdly, heat the mixer and keep it at 150 °C, pour the heated coarse and fine aggregate and asphalt into the mixer in turn and mix for 1~1.5 min; suspend mixing, add the heated mineral powder and continue mixing until it is even, and the total mixing time is 3 min. Fourthly, put the mixture into the mold and compact it with a rotary compactor at a compaction temperature of 145 °C. Finally, demold the specimen and place it in the natural environment to cool down.

The production process of the PAC13 was the same as that for the AC13.

Cylinder samples were made with a diameter of 150 mm and a height of 170 mm. All specimens were placed in a sunny and dry place for seven days before they were tested. Each specimen was attached to 3 thermal sensors by drilling holes in it, which were located in the center of the sections 1, 8.5 and 16 cm below the top surface. Figure 1 illustrates the locations of the thermal sensors.

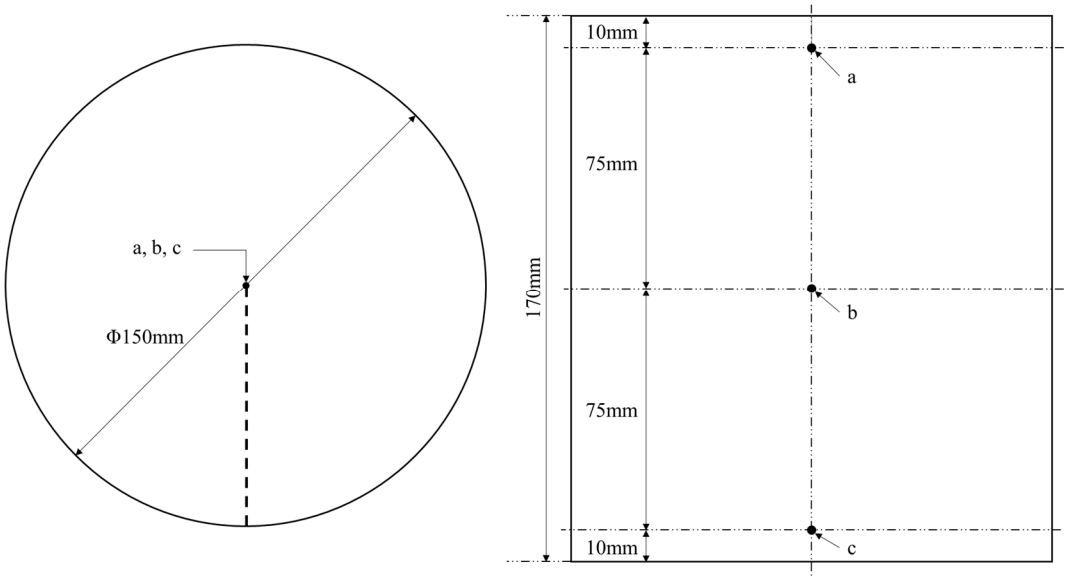

Figure 1. Schematic diagram of sensor locations (left: plane view; right: front view; sites a, b, c are the location of thermal sensors).

The DS18B20 digital temperature sensor was selected to monitor the air temperature and the temperature inside the specimens. As shown in Figure 2, sensors at site a, site b and site c were used to measure the temperature of the upper part, the middle part and the bottom part of the specimen, respectively. At the designated height of the specimens, holes were drilled from the side of the specimens in the direction perpendicular to the axis. The drilling depth was 75mm, and the drilling diameter was slightly larger than the outer diameter of the sensor probe. The temperature sensor probe was put in the designated position, and then the gap between the drilling hole and the data line was sealed with epoxy resin. At the same time, a temperature sensor was placed above the specimens in the test to measure the air temperature. All the 10 temperature sensors were connected in parallel and connected to a computer via an RS485 converter. In addition, a Fluke Ti10 thermal imager and an irradiometer were employed to measure the surface temperature of the specimens and the intensity of solar radiation, respectively.

Figure 2. Wrapped specimens with side and bottom thermal insulated (left: dense asphalt concrete or AC13; middle: porous asphalt concrete or PAC13; right: cement concrete or C25).

The sides and bottom of all the three specimens were wrapped with thermal insulation to avoid heat transfer from these locations. Figure 2 depicts the wrapped and instrumented specimens. The wrapped and instrumented specimens were placed in an open field with natural sunlight and kept a certain distance from each other. Firstly, the specimens were placed in the open field for a week to reach a balance in the environment. Then the temperature monitoring started.

The air temperature, the solar radiation intensity and the temperature of the surface, the upper part, the middle part and the bottom part of the specimens were monitored in the test. The test system automatically recorded the temperature data obtained by the temperature sensors each 10 min. The surface temperature and the solar radiation intensity were also measured by the infrared thermal imager and the irradiometer, respectively, every hour during the test period. The test period was divided into cycles of 24 h and the test results of each cycle with stable outdoor conditions and complete data records were selected for further analysis.

3. Results

3.1. Temperature Variation of the Pavement Materials due to the Natural Environment

3.1.1. Temperature Distribution

The original recorded data of the temperature and solar radiation intensity as shown in Table S1. Figure 3a–c illustrates the air temperature change, the solar radiation intensity change, and the temperature change of the surface, the upper part, the middle part and the bottom part of the specimens in a typical cycle. As can been seen, the temperature of the surface and the upper part was higher

than the air temperature throughout the test cycle for all the three materials. The temperature of the middle and the bottom parts was lower than that of the air in the morning. During daytime, the surface temperature was the highest and the temperature decreased gradually with the increase of depth. The air temperature started to decrease when the solar radiation intensity became weak and reached a low level quickly, while the temperature of the materials decreased at a relatively low rate. At night, the temperature of the upper part was slightly lower than that of the middle and the bottom for all the three materials. However, the surface temperature had more fluctuations.

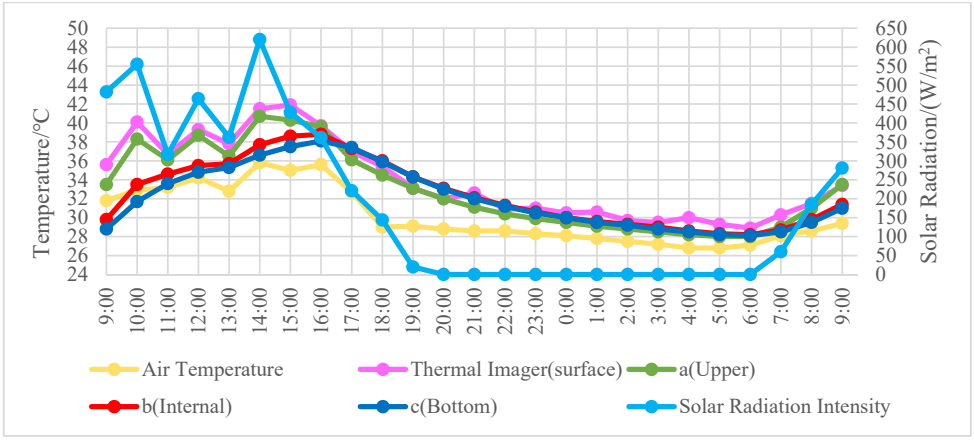

(**a**)

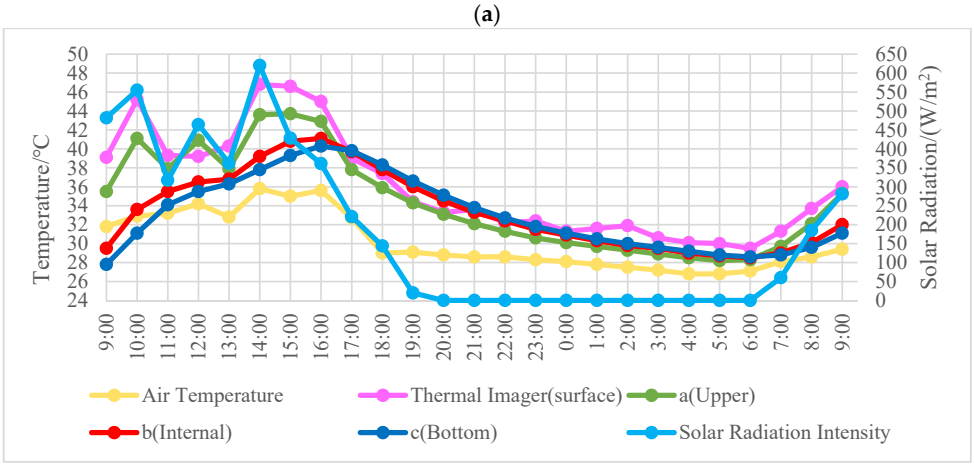

(**b**)

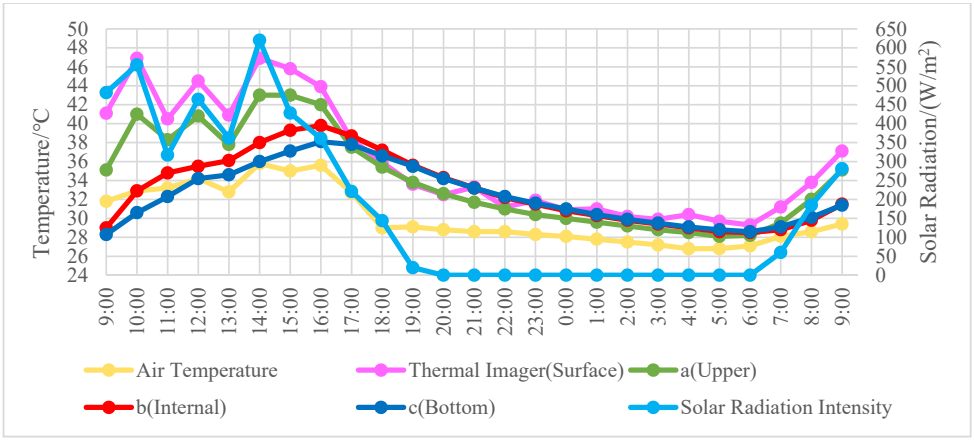

(**c**)

Figure 3. Temperature distribution of the pavement materials: (**a**) C25; (**b**) AC13; (**c**) PAC13.

The variation trends of the temperatures were similar to that of the solar radiation during daytime, while the variation was relatively gentle at night when there was no influence of the solar radiation. The temperature of pavement materials is very sensitive to the changes of the natural environment, especially the surface temperature, which can be significantly affected by the change of solar radiation during daytime.

The temperature range in the test cycle at each location was calculated for all the three materials, which is helpful to compare the effects of the natural environment on the three materials. Table 5 lists the temperature range of each location.

Table 5. Temperature range of the specimens and natural environments.

Monitoring Object		Max	Min	△
Air temperature		35.8 °C	26.8 °C	9.0 °C
Thermal imager (surface)	C25	41.9 °C	28.9 °C	13.0 °C
	AC13	46.8 °C	29.5 °C	17.3 °C
	PAC13	46.9 °C	29.3 °C	17.6 °C
a(Upper)	C25	40.7 °C	28.0 °C	11.3 °C
	AC13	43.7 °C	28.2 °C	15.5 °C
	PAC13	43.0 °C	28.1 °C	14.9 °C
b(Internal)	C25	38.8 °C	28.2 °C	10.6 °C
	AC13	40.1 °C	28.5 °C	11.6 °C
	PAC13	39.8 °C	28.5 °C	11.3 °C
c(Bottom)	C25	38.1 °C	28.1 °C	10.0 °C
	AC13	40.3 °C	27.2 °C	13.1 °C
	PAC13	38.1 °C	28.3 °C	9.8 °C
Solar Radiation Intensity		620.0 W/m^2	0	620.0 W/m^2

As shown in Table 5, the temperature range at any location of the specimens was larger than the air temperature range. In general, the temperature change of all materials decreased with the increase of depth, except for dense asphalt concrete, whose temperature change at the bottom was greater than that in the middle. Among the three materials, the temperature range of the cement concrete was lower than that of the other two materials at any location except at the bottom, where the temperature range of the porous asphalt concrete was smaller than that of the cement concrete. In the daytime, the heat absorbed and surface temperature of the specimens were mainly affected by the solar radiation absorption rate. The higher the absorptivity of the materials, the more heat they get from the solar radiation and the same applies to the surface temperature. The order of the solar radiation absorptivity of the three materials was AC13 ≈ PAC13 > C25. So, the surface temperature of the dense asphalt concrete was the highest of the three materials and it got the most heat from the sun radiation. At night, when the specimens were exothermic by thermal radiation, the order of the thermal radiation coefficient of the three materials was AC13 ≈ PAC13 > C25. The higher the surface temperature, the higher the radiation intensity and the faster the cooling rate. The heat transfer in the internal structure of the pavement was mainly realized by heat conduction. In the daytime, the surface of the road absorbs heat and transmits it to the lower structural layers through heat conduction, which causes the overall temperature of the road to rise. At night, the surface temperature decrease in the lower part of the road is relatively high, and the heat is transferred to the upper part of the road. The important thermal physical parameter related to the heat conduction process is thermal diffusivity of the material. Thermal diffusivity can be calculated by the thermal conductivity, density and specific heat capacity. The order of the solar radiation absorptivity of the three materials was AC13 > PAC13 > C25. So, the temperature change of dense asphalt concrete was the most significant in a test cycle. It absorbed the most heat during the day and released the most heat at night.

3.1.2. Correlation between materials temperature and environment factors

Correlation coefficient r(X,Y) is a statistical index used to represent the relationship between two variables, which is defined as Equation (1).

$$rX,Y = \frac{\sum(x-\overline{x})(y-\overline{y})}{\sqrt{\sum(x-\overline{x})^2\sum(y-\overline{y})^2}} \quad (1)$$

where X, Y are two variables, x is the value of the variable X, $\overline{x}$ is the average value of variable X; y is the value of the variable Y and $\overline{y}$ is the average value of variable Y.

Figure 4a–d depicts the relationship between the pavement materials temperature and the air temperature at the same time. Figure 5a–d depicts the relationship between the pavement materials temperature and the solar radiation intensity at the same time.

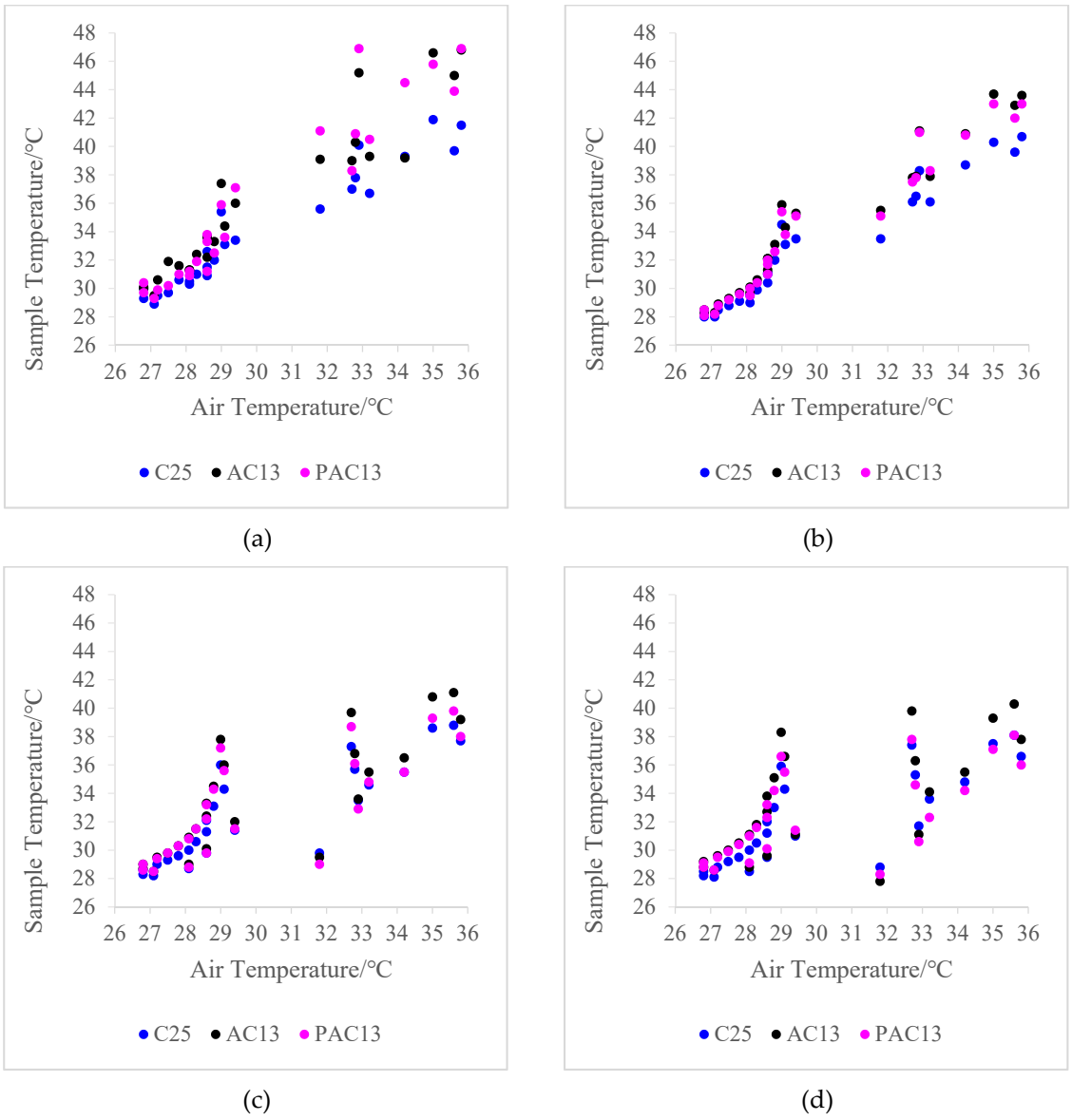

Figure 4. Relationship of pavement material temperature with air temperature: (**a**) thermal imager (surface); (**b**) a(upper part); (**c**) b(middle); (**d**) c(bottom).

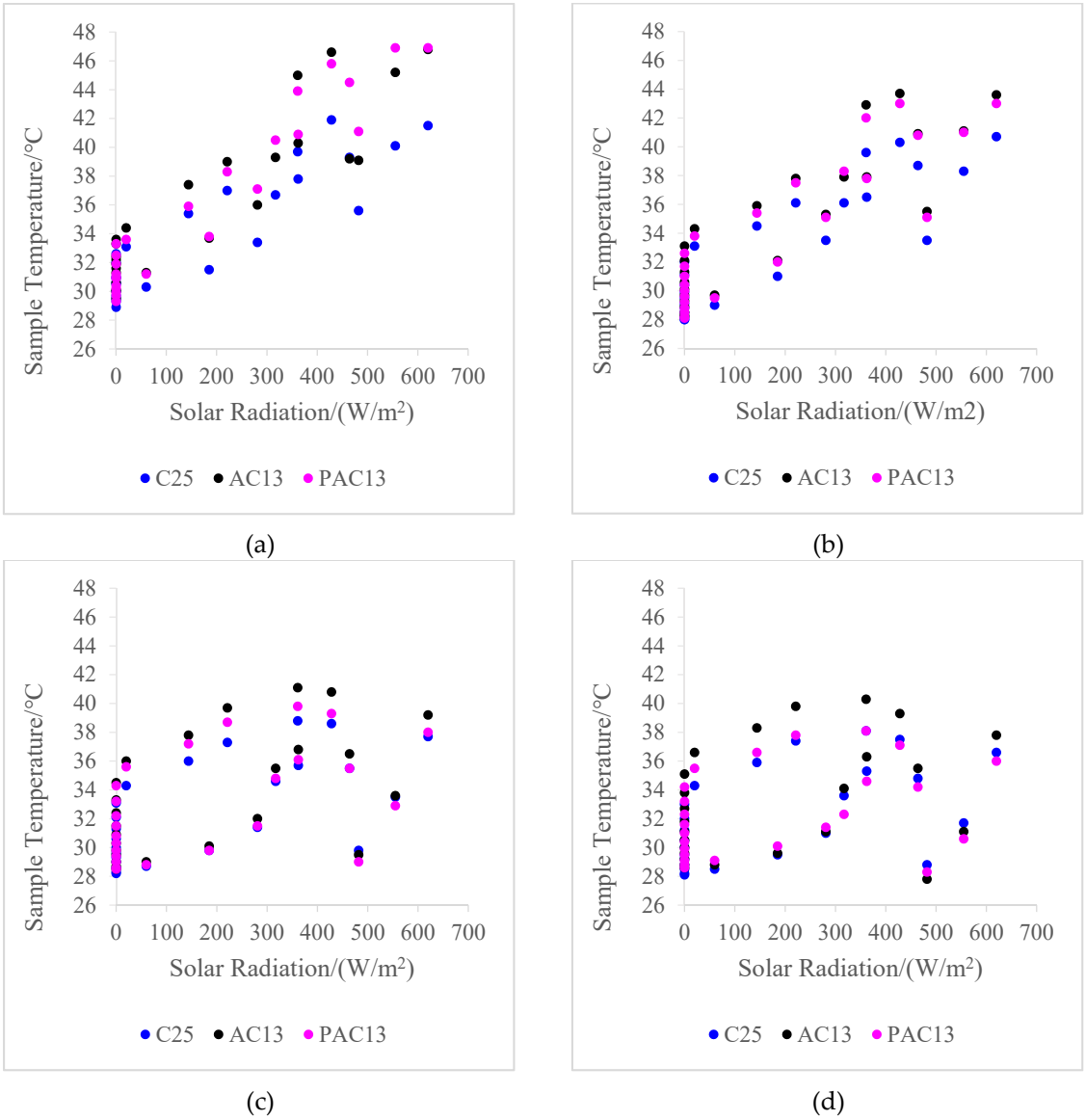

Figure 5. Relationship of pavement material temperature to solar radiation intensity: (**a**) thermal imager (surface); (**b**) a(upper part); (**c**) b(middle); (**d**) c(bottom).

As shown in Figure 4, the temperature of pavement materials has positive correlation with the air temperature to different extents at different depths. The correlation at low temperature level is stronger than that at high temperature level, which may be attributed to the different effect of solar radiation, and the correlation tends to be poor with increasing depth.

As shown in Figure 5, the temperature variation at surface positively correlates with the solar radiation intensity but that at the middle and bottom has poor correlation to the solar radiation.

The test cycle was divided into two sections, 6:00–19:00 (daytime) and 19:00–6:00 (night) to discriminate between the different effects of solar radiation during daytime and night. According to Equation (1), the correlation coefficients between the temperature of the three pavement materials and environmental factors, including the air temperature and the solar radiation intensity, are calculated for the whole cycle and each time section. The results are listed in Table 6.

Table 6. Correlation coefficient between pavement material temperatures and environmental conditions.

Correlation Coefficient	Material Type	Thermal Imager (Surface)	a(Upper Part)	b(Middle)	c(Bottom)
$r(T_{Air}, T_k)$	C25	0.9672	0.9679	0.8618	0.8020
	AC13	0.9536	0.9686	0.8191	0.6948
	PAC13	0.9582	0.9707	0.7900	0.6648
$r_{daytime}(T_{Air}, T_k))$	C25	0.9465	0.9484	0.7933	0.7159
	AC13	0.9204	0.9470	0.7441	0.6146
	PAC13	0.9306	0.9499	0.7154	0.5762
$r_{night}(T_{Air}, T_k)$	C25	0.8726	0.9466	0.9429	0.9464
	AC13	0.9104	0.9532	0.9488	0.9432
	PAC13	0.8609	0.9577	0.9509	0.9563
$r_{daytime}(S, T_k)$	C25	0.8467	0.8059	0.4534	0.3368
	AC13	0.8568	0.8180	0.3708	0.1971
	PAC13	0.9438	0.8293	0.3340	0.1690

In the whole cycle, the correlation coefficients between pavement material temperature and air temperature were relatively high and show a decreasing trend with increasing depth. In terms of different time sections, the correlation coefficients between pavement material temperature and air temperature were all above 0.85 at night for all the three materials, while they were all lower than 0.8, even 0.6, at the middle and bottom at daytime though they were all above 0.9 at upper part and surface. It is shown that the correlation between pavement material temperature and air temperature at night is stronger than that during daytime. This is because there is solar radiation during daytime, which has a great impact on the surface temperature, thus decreasing the correlation between the pavement material temperature and air temperature.

The correlation coefficients between solar radiation intensity and pavement material temperature at the surface and the upper part were all above 0.8 while those at the middle and bottom were all lower than 0.5. It is shown that solar radiation has a dominant effect on the temperature of the materials near the surface.

3.2. Heat Island Potentials of Different Pavement Materials

3.2.1. Distribution of Heat Island Potential

Heat island potential (HIP) as a quantitative indicator was proposed to evaluate the effect of pavement materials on UHIE at specific times and specific locations, which is defined as Equation (2).

$$HIP_{k,i} = \frac{T_{k,i}}{T_{Air,i}} \times 100\% = \frac{T_{k,i} - T_{Air,i}}{T_{Air,i}} \times 100\% \quad (2)$$

where $HIP_{k,i}$ is heat island potential of each hour at different depths; $T_{Air,i}$ is the air temperature at i hour, $i = 9,\ 10, \cdots 23,\ 0, \cdots 9$; $T_{k,i}$ is the material temperature at different depths, k is a, b or c.

Figure 6a–d illustrates the heat island potentials at different moments and different depths. As shown in Figure 6, the UHIE is more intense during daytime. The UHIE will continue at night though there is no solar radiation. The closer to the surface, the greater the contribution of the material to the UHIE. The materials at middle and bottom may not contribute to the UHIE in the early morning.

According to the Figure 6, at any time and at any depth the HIP value of asphalt concrete is higher than that of cement concrete. So compared to cement concrete, the two asphalt materials show significantly high potential to create the UHIE.

Inside the pavement structure, porous asphalt concrete has a greater impact on UHIE than dense asphalt concrete at most times of the day. As for the road surface, in the morning when the pavement surface is heated rapidly due to the absorption of solar radiation, porous asphalt concrete has a greater impact on UHIE than dense asphalt concrete.

3.2.2. Accumulated Heat Island Potential

As mentioned above, the heat island potential of pavement materials may be different at different times. So, it is necessary to define a quantitative indicator for describing the total heat island potential of a material. The accumulated heat island potential (HIP_k) was proposed, which can be calculated according to Equation (3).

$$HIP_k = \frac{\int T_k(t)dt}{\int T_{Air}(t)dt} \times 100\% = \frac{\int |T_k(t) - T_{Air}(t)|dt}{\int T_{Air}(t)dt} \times 100\% = \frac{\sum_{i=1}^{24} |T_{k,i} - T_{Air,i}|}{\sum_{i=1}^{24} T_{Air,i}} \times 100\% \quad (3)$$

where HIP_k is the accumulated heat island potential at different locations.

Figure 7 depicts the accumulated heat island potential of the three pavement materials at different locations. It is shown that the trend of HIP with the depth of pavement is the same for all the three pavement materials. The HIP decreases with increasing depth. The highest HIP emerges at the surface and the smallest HIP occurs at the bottom.

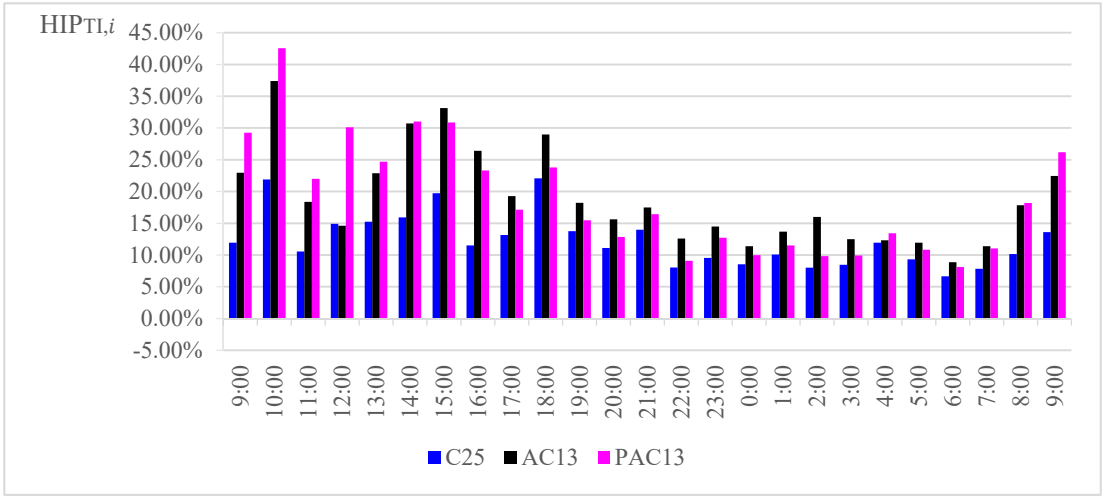

(a)

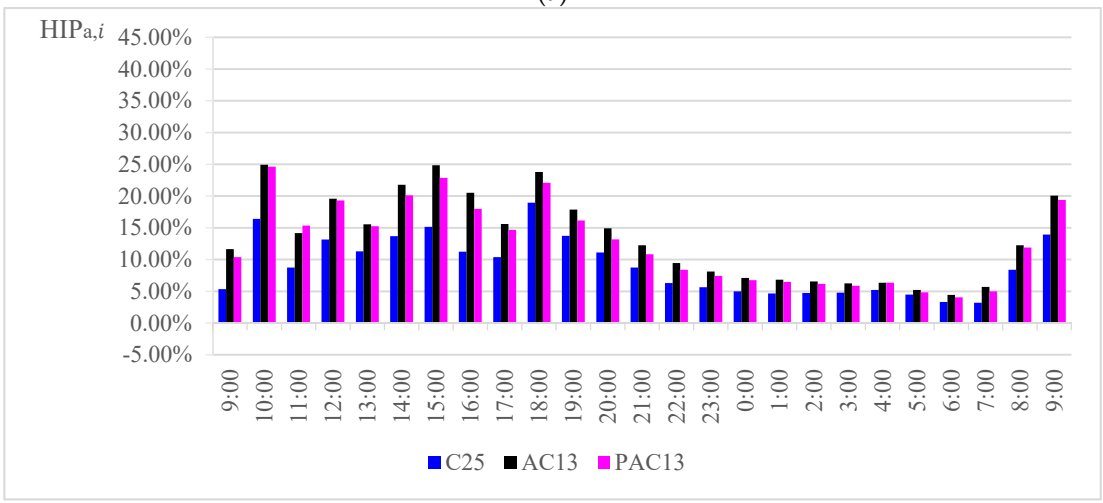

(b)

Figure 6. *Cont.*

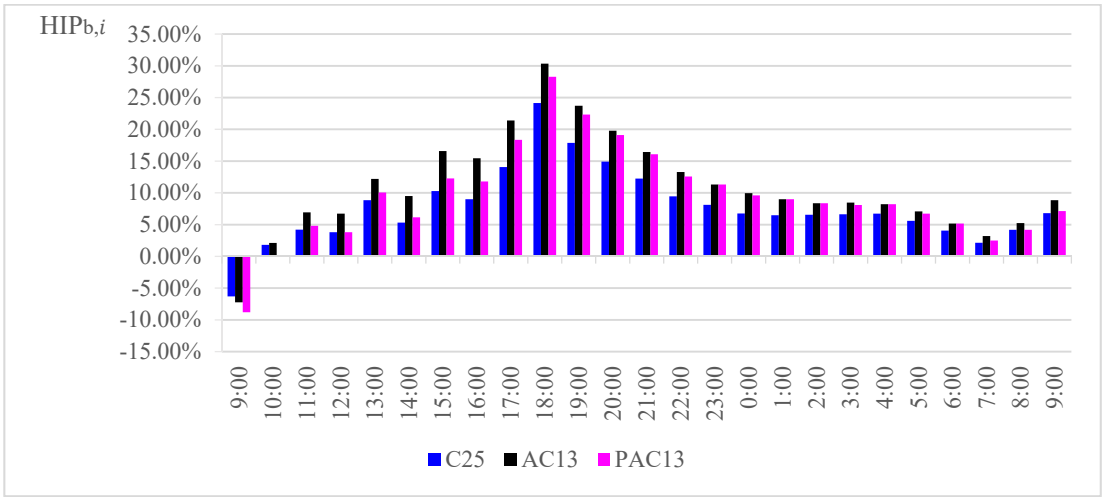

(c)

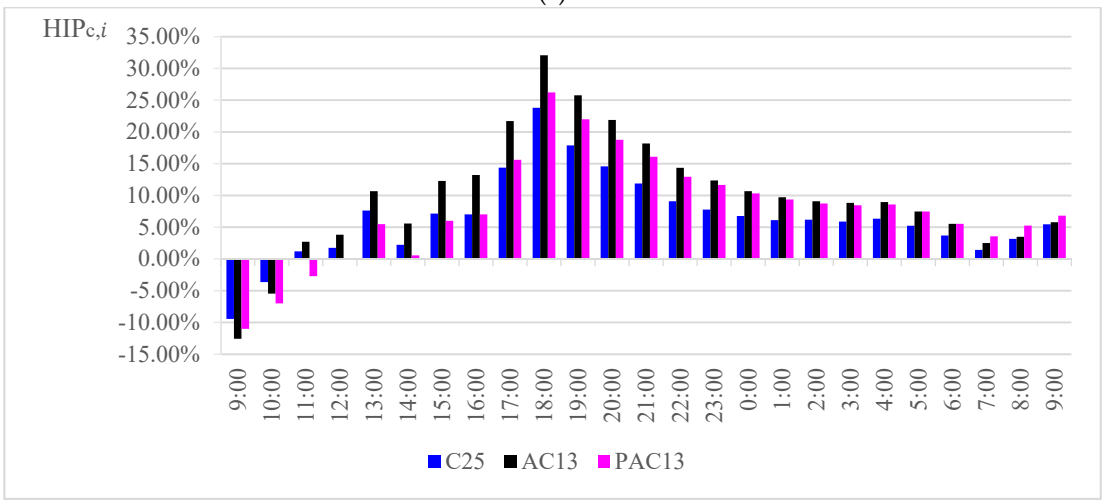

(d)

Figure 6. Distribution of heat island potential: (**a**) surface (by thermal imager); (**b**) a (upper part); (**c**) b(middle); (**d**) c(bottom).

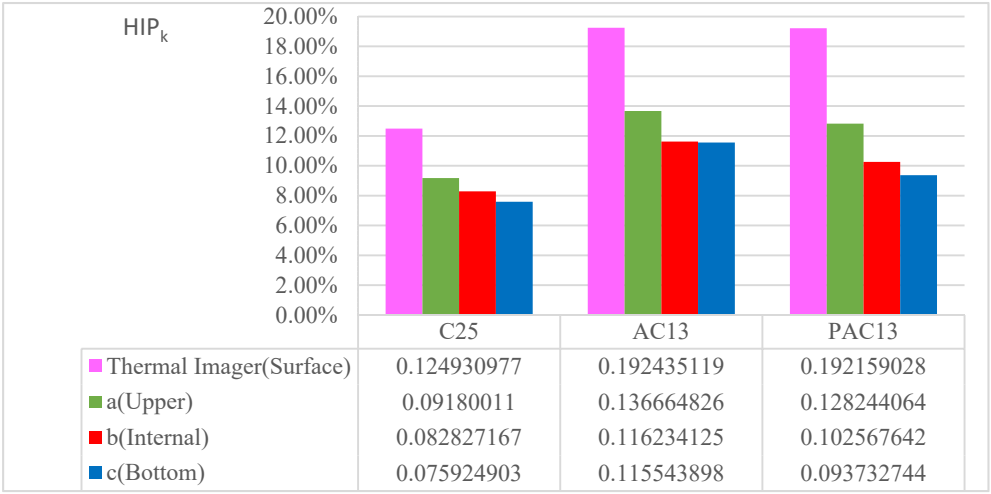

	C25	AC13	PAC13
Thermal Imager(Surface)	0.124930977	0.192435119	0.192159028
a(Upper)	0.09180011	0.136664826	0.128244064
b(Internal)	0.082827167	0.116234125	0.102567642
c(Bottom)	0.075924903	0.115543898	0.093732744

Figure 7. Accumulated heat island potential.

The total accumulated heat island potential is 0.376, 0.605 and 0.517 for the cement concrete, the dense asphalt concrete and the porous asphalt mixture, respectively. The cement concrete shows better anti-UHIE properties; its total accumulated heat island potential is only 62.1% of the dense asphalt concrete and 72.7% of the porous asphalt mixture. The porous asphalt mixture also shows some advantages for anti-UHIE; its total accumulated heat island potential is 14.5% lower than that of the dense asphalt concrete.

3.3. Heat Energy Absorption and Release of Materials in One Cycle

The direct measurement of pavement materials' heat island effect is heat energy absorption and release. Using heat capacity analysis, one can calculate the amount of heat energy a specimen absorbs and emits energy in a day–night cycle.

According to the experimental results presented in the previous section, most of the time, the temperature of site b is between those at site a and site c. To simplify the calculation, one can use the average temperature of the specimen according to Equation (4)

$$T_{avg} = \frac{T_a + T_b + T_c}{3} \tag{4}$$

where T_a is the temperature at site a; T_b is the temperature at site b; T_c is the temperature at site c.

The data of the average temperature and solar radiation are shown in Table S2. Figure 8 presents the time variation of the average temperature and solar radiation. It can be seen from Figure 8 that the variation of the average temperatures of the three specimens has the same trend, which depends the solar radiation intensity and the temperature status of the specimens. Whether the material absorbed or released heat energy not only depended on the solar radiation intensity but also related to the temperature status of the material. The higher the temperature of the material is, the faster the heat was released. The stronger the solar radiation, the faster the heat absorption. The overall heat absorption or heat release is determined by both. The temperature of cement concrete was lower than those of the asphalt concrete mixtures. The temperature of porous asphalt concrete was lower than that of the dense asphalt concrete. In terms of temperature, the asphalt concrete may have more effect on the UHIE, and the effect is smaller with increasing porosity.

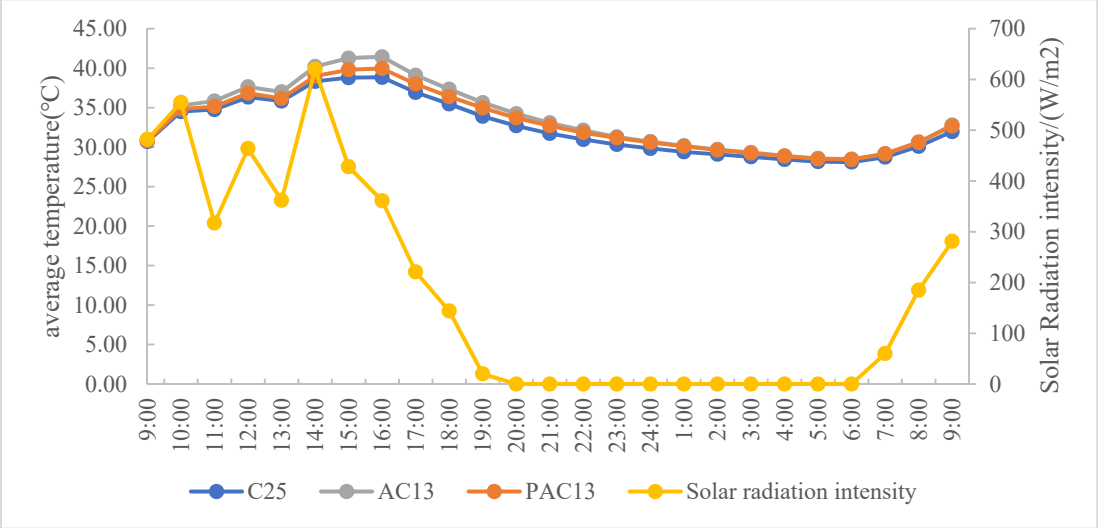

Figure 8. Average temperature and solar radiation intensity with time.

A more rational measurement parameter might be the energy absorbed or released by the specimen, which is related to the change of temperature and can be calculated by Equation (5):

$$Q = CmT \tag{5}$$

where C is the specific heat capacity; m is the mass of the specimen; T is the temperature variation.

The average specific heat and density of the three materials [28] are presented in Table 7.

Table 7. Specific heat and density of the three materials.

Specimen Type	Density (g/cm^3)	Specific Heat Capacity (J/kg·K^{-1})
Cement concrete	2.380	960
Porous asphalt concrete	2.121	850
Dense asphalt concrete	2.408	850

Using the specific heat capacity and density, and the temperature of each hour, variation of the specimen heat energy at each hour was calculated and shown in Figure 9. If the value is positive, it means that the material absorbed heat energy. If the value is negative, it emitted heat energy.

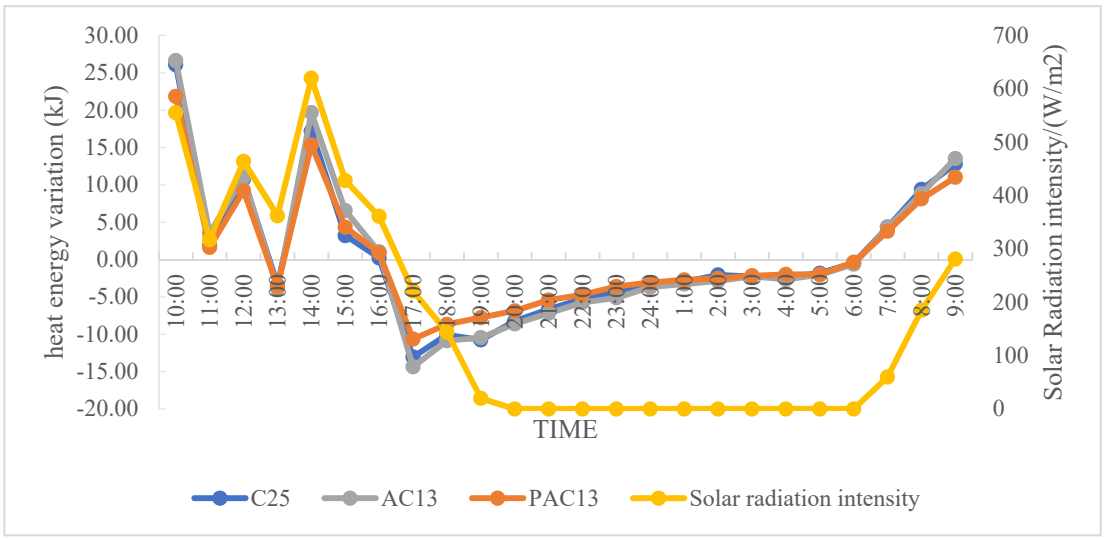

Figure 9. Heat energy change of the specimens per hour.

The data of heat energy change per hour are shown in Table S2. From Figure 9, it is clear that the trends of heat absorption and heat release of the three materials are consistent and closely related to the solar radiation intensity. The heat absorption and heat release rate of dense asphalt concrete was the fastest among the three materials. It is also clear that by increasing the porosity of asphalt mixture, the rate can be effectively reduced.

The experimental period was from 9:00 a.m. to 9:00 a.m. the next day. Figure 9 shows that there were three stages of heat change in a test cycle. In the first stage, from 9:00 a.m. to 4:00 p.m., the heat absorption process was the main process. In the second stage, from 4:00 p.m. to 6:00 a.m. of the next day, the exothermic process was the main process. In the third stage, after 6:00 a.m. of the next day, the heat absorption process became the main process. By adding the energy of each hour in different stages, we can get the change of thermal energy in this stage. The total heat absorption Q_{absorb} in this experimental period can be obtained by adding up the energy changes in the first and third stages, and the energy change of the second stage is the total heat released $Q_{release}$ in the experimental period. Results are shown in Table 8.

Table 8. Maximum range of temperature and heat energy variation.

Specimen	T_{max}(°C)	T_{min}(°C)	Q_{absorb}(kJ)	$Q_{release}$(kJ)
C25	38.83	28.10	82.37	−73.67
AC13	41.43	28.47	91.21	−79.73
PAC13	39.97	28.43	72.57	−62.46

According to Table 8, which compares the heat absorbed and released by three materials in one cycle, the order of heat absorption capacity was AC13 > C25 > PAC13 and the order of heat release capacity was also AC13 > C25 > PAC13. The results have shown that dense asphalt concrete pavements have more effect on the UHIE than cement concrete. Porous asphalt pavements have less effect than dense asphalt concrete. The results of thermodynamic analysis are consistent with the index HIP.

4. Conclusions

This paper presents a study focusing on the potential of pavement materials to contribute to the UHIE. Three typical pavement materials, a cement concrete, a dense asphalt concrete and a porous asphalt mixture, were selected for evaluation in an open field for their anti-UHIE properties. Some conclusions can be drawn as follows.

(1) The temperature inside pavement specimens distinctly depends on the depth, which varies with the air temperature but is mostly higher than it. The temperature at surface is the highest, followed by that at the upper part, the middle part and the bottom part. After the solar radiation is absorbed by the pavement, the pavement transmits the heat to the air through radiation, conduction and convection, which is the main source of heat in the air. The solar radiation directly absorbed by the atmosphere makes the effect of air heating very small. Generally, the pavement surface temperature will be higher than the air temperature

(2) The temperature of pavement specimens at the upper part is highly sensitive to environmental conditions. The solar radiation in the daytime significantly correlates to the temperature of pavement surface and the upper part. The correlation becomes weak at the middle and bottom of the pavement specimens.

(3) The heat island potentials of pavement materials can be effectively evaluated by the indicators of $HIP_{k,i}$ and HIP_k, and the lower values of them show better anti-UHIE performance of the materials. Among the three materials tested in this paper, the anti-UHIE performance of cement concrete is significantly higher than that of the asphalt mixtures, and the porous asphalt mixture is slightly better than the dense asphalt concrete in anti-UHIE.

The results derived from this study are preliminary but show it is feasible to use the proposed approach to estimate the UHIE of different pavement materials. HIP is obtained by analyzing the data of materials' internal and environmental temperature and solar radiation. It is relatively convenient to be used in long-term temperature monitoring in engineering. In future research, we will use HIP to analyze the impact of various climate events on the long-term characteristics of UHIE and verify the reliability of HIP analysis. In addition, data-based analysis methods can consider more environmental factors such as air humidity and material moisture content, which are not difficult to obtain, and will optimize the calculation method of HIP.

Supplementary Materials: The following are available online at http://www.mdpi.com/2071-1050/12/11/4752/s1, Table S1 The Original Recorded Data of the Temperature and solar Radiation Intensity, Table S2 The Data in Figures 8 and 9.

Author Contributions: Conceptualization, H.Y. and L.W.; formal analysis, Y.M.; funding acquisition, H.Y.; methodology, H.Y. and Y.M.; validation, K.Y.; writing – original draft, C.Y.; writing – review & editing, H.Y., Y.M. and L.W. All authors have read and agreed to the published version of the manuscript.

Funding: This research was funded by the China Postdoctoral Science Foundation (2019M660467) and the Fundamental Research Funds for the Central Universities (FRF-TP-18-048A1).

Conflicts of Interest: The authors declare no conflict of interest.

References

1. Esra, T.T. Recycling of marble waste: A review based on strength of concrete containing marble waste. *J. Environ. Manag.* **2019**, *231*, 86–97.
2. Woszuk, A.; Wróbel, M.; Franus, W. Influence of Waste Engine Oil Addition on the Properties of Zeolite-Foamed Asphalt. *Materials* **2019**, *12*, 2265. [CrossRef] [PubMed]
3. Woszuk, A.; Wróbel, M.; Franus, W. Application of Zeolite Tuffs as Mineral Filler in Warm Mix Asphalt. *Materials* **2020**, *13*, 19. [CrossRef] [PubMed]
4. Pomerantz, M.; Akbari, H.; Chen, A.; Taha, H.; Rosenfeld, A.H. Paving materials for heat island mitigation. In Proceedings of the 1998 ACEEE Summer Study on Energy Efficiency in Buildings, Pacific Grove, CA, USA, 23–28 August 1998; Volume 9, p. 135.
5. Zhou, B.; Rybski, D.; Kropp, J.P. On the statistics of urban heat island intensity. *Geophys. Res. Lett.* **2013**, *40*, 5486–5491. [CrossRef]
6. Zhou, B.; Rybski, D.; Kropp, J.P. The role of city size and urban form in the surface urban heat island. *Sci. Rep.* **2017**, *7*, 4791. [CrossRef] [PubMed]
7. Rizwan, A.M.; Dennis, L.Y.; Liu, C. A review on the generation, determination and mitigation of urban heat island. *J. Environ. Sci.* **2008**, *20*, 120–128. [CrossRef]
8. Bornstein, R.; Lin, Q. Urban heat islands and summertime convective thunderstorms in atlanta: Three case studies. *Atmos. Environ.* **2000**, *34*, 507–516. [CrossRef]
9. Dixon, P.G.; Mote, T.L. Patterns and causes of atlanta's urban heat island initiated precipitation. *J. Appl. Meteorol.* **2003**, *42*, 1273–1284. [CrossRef]
10. Santamouris, M. On the energy impact of urban heat island and global warming on buildings. *Energy Build.* **2014**, *82*, 100–113. [CrossRef]
11. Santamouris, M.; Cartalis, C.; Synnefa, A.; Kolokotsa, D. On the impact of urban heat island and global warming on the power demand and electricity consumption of buildings—A review. *Energy Build.* **2015**, *98*, 119–124. [CrossRef]
12. Morini, E.; Touchaei, A.G.; Castellani, B.; Rossi, F.; Cotana, F. The impact of albedo increase to mitigate the urban heat island in terni (italy) using the wrf model. *Sustainability* **2016**, *8*, 999. [CrossRef]
13. Hassid, S.; Santamouris, M.; Papanikolaou, N.; Linardi, A.; Klitsikas, N.; Georgakis, C.; Assimakopoulos, D.N. The effect of the athens heat island on air conditioning load. *Energy Build.* **2000**, *32*, 131–141. [CrossRef]
14. Hondula, D.M.; Georgescu, M.; Balling, R.C. Challenges associated with projecting urbanization-induced heat-related mortality. *Sci. Total Environ.* **2014**, *490*, 538–544. [CrossRef] [PubMed]
15. Deilami, K.; Kamruzzaman, M.; Liu, Y. Urban heat island effect: A systematic review of spatio-temporal factors, data, methods, and mitigation measures. *Int. J. Appl. Earth Obs. Geoinf.* **2018**, *67*, 30–42. [CrossRef]
16. Ai-Min, S.; Wei, J. Design philosophy and architecture of eco-friendly porous pavement materials. *China J. Highw. Transp.* **2018**, *31*, 1–6.
17. Zhang, X.; Kong, Y.J.; Guan, Y.B. Analysis of the effect of asphalt pavement on heating community atmosphere. *J. Jinling Inst. Technol.* **2006**, *22*, 16–18. [CrossRef]
18. Jia, L.; Sun, L.; Huang, L.; Qin, J. A numerical temperature prediction model for asphalt concrete pavement. *J. Tongji Univ.* **2007**, *35*, 1039.
19. Yang, X.; Yang, X.; Ding, J.; Yang, M.; Jiang, R. Heat transfer of the concrete thermal storage system. *J. Dongguan Univ. Technol.* **2012**, *19*, 70–74. [CrossRef]
20. Bretz, S.; Akbari, H.; Rosenfeld, A. Practical issues for using solar-reflective materials to mitigate urban heat islands. *Atmos. Environ.* **1997**, *32*, 95–101. [CrossRef]
21. Kinouchi, T.; Yoshinaka, T.; Fukae, N.; Kanda, M. Development of cool pavement with dark colored high albedo coating. *Target* **2003**, *50*, 40.
22. Hamdami, N.; Monteau, J.Y.; Bail, A.L. Simulation of coupled heat and mass transfer during freezing of a porous humid matrix. *Int. J. Refrig.* **2004**, *27*, 595–603. [CrossRef]
23. Hopstock, D.M.; Zanko, L.M. *Minnesota Taconite as a Microwave-Absorbing Road Aggregate Material for Deicing and Pothole Patching Applications*; Natural Resources Research Institute, University of Minnesota Duluth: Duluth, MN, USA, 2005.

24. Asaeda, T.; Ca, V.T. Characteristics of permeable pavement during hot summer weather and impact on the thermal environment. *Build. Environ.* **2000**, *35*, 363–375. [CrossRef]
25. Hall, M.; Allinson, D. Analysis of the hygrothermal functional properties of stabilised rammed earth materials. *Build. Environ.* **2009**, *44*, 1935–1942. [CrossRef]
26. Santos, G.H.D.; Mendes, N. Heat, air and moisture transfer through hollow porous blocks. *Int. J. Heat Mass Transf.* **2009**, *52*, 2390–2398. [CrossRef]
27. Yang, J.; Jiang, G. A study on strength of pervious concrete as pavement material. *China Concr.* **2000**, *10*, 27–30.
28. Yang, K. Analysis of Three Typical Pavement Affecting Urban Heat Island. M.D. Thesis, University of Science and Technology Beijing, Beijing, China, 2018.